An Integrated Asian Emission Inventory and Analysis of its Characteristics in Support of TRACE-P and ACE-Asia

J.-H. Woo, D.G. Streets, G.R. Carmichael, Y. Tang, T.C. Bond, J. Dorwart, S. Pinnock, Q. Fu, K.F. Yarber, G. Kurata, N. Thongboonchoo, A. White

Center for Global and Regional Environ. Research, Univ. Iowa, USA
Argonne National Laboratory, USA
National Center for Atmospheric Research, Boulder, CO
Global Vegetation Monitoring, World Fire Web, EC JRC, Italy
Department of Ecological Engineering, Toyohashi University of Technology, Japan
Department of Chemical Engineering, University of California, USA

Development Methodology

Definition of the inventory domain, its constituent countries, international shipping lanes, and sub-regions

An inventory of air pollutant emissions in Asia in the year 2000 is developed to support atmospheric modeling and analysis of observations taken during the TRACE-P and the ACE-Asia experiment.

We estimate total Asian emissions as follows: 34.3 Tg SO_2, 26.8 Tg NO_x, 9870 Tg CO_2, 279 Tg CO, 107Tg CH_4, 52.2 Tg NMVOC, 2.54Tg black carbon (BC), 10.4 Tg organic carbon (OC), and 27.5 Tg NH_3. In addition, NMVOC are speciated into 19 subcategories according to functional groups and reactivity. Thus, we are able to identify the major source regions and types for many of the significant gaseous and particle emissions that influence pollutant concentrations in the vicinity of the TRACE-P and ACE-Asia field measurements

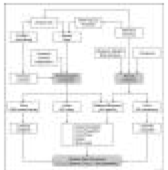

Schematic methodology for the development of Asian emission estimates

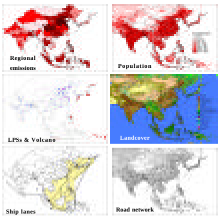

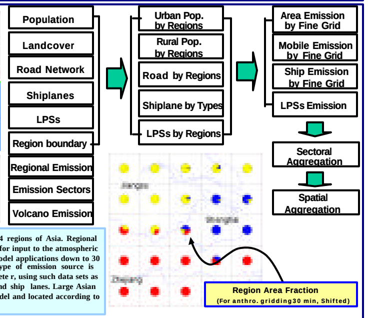

The anthropogenic emissions are initially calculated for 64 regions of Asia. Regional emissions are then gridded at a variety of spatial resolutions for input to the atmospheric simulation models, ranging from 1°×1° for most regional model applications down to 30 sec × 30 sec resolution for urban-scale studies. Each type of emission source is represented by a different spatially resolved surrogate parameter, using such data sets as urban and rural population, road networks, land cover, and ship lanes. Large Asian power plants are separately identified in the RAINS-Asia model and located according to their latitude/longitude coordinates.

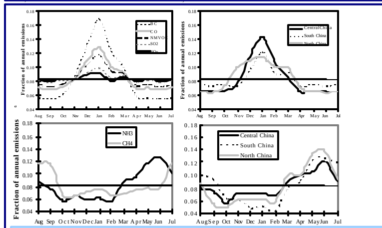

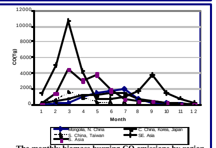

The monthly biomass burning CO emissions by region

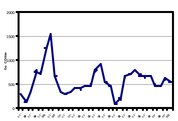

The daily biomass burning CO emissions (March, Year 2001)

Emissions are initially calculated for an annual time period. However, it is recognized that there is considerable seasonal variation for some species, associated with such activities as the burning of fossil fuels for home heating in winter and the temperature dependence of releases of NH_3 from fertilizer application and CH_4 from manure. Biomass burning clearly has a very high degree of seasonality, determined by local agricultural practices and meteorological conditions. Such seasonality is important in preparing emissions for comparison with time-specific field experiments. For this reason we have apportioned annual emissions to daily and monthly emissions using a variety of techniques.

The techniques used to develop biomass burning estimates are elaborate and based on national surveys of fires, AVHRR satellite fire counts, and TOMS AI data. Efforts concentrated on realistically apportioning annual emissions to the months of March and April, which correspond to the timing of the TRACE-P and ACE-Asia field campaigns.

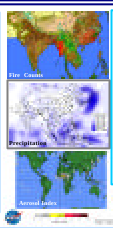

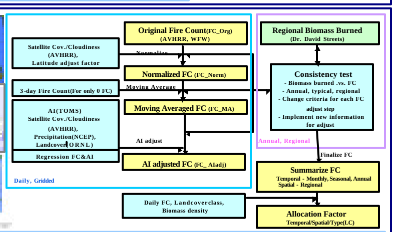

We used the annual-regional emission data from Yarber et al. [manuscript in preparation, 2002] to estimate daily emissions for the period from Feb 26 to May 10, 2001. These estimates of total biomass burning emissions by regions were further analyzed to produce daily fire events. The AVHRR fire count, cloud, and satellite coverage data was used to analyze daily fire events. The basic allocation method was to distribute the emissions within a region in time and space according to the daily fire count statistics normalized by the total number of detected fires.

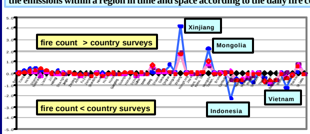

Comparison of country surveys with various AVHRR fire-count adjustments reveals problem areas for further investigation

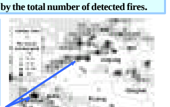

Fire detection from Xinjiangand Pakistan could be flares from Oil/Gas drilling site

Landcover Fraction estimation to allocate type of burning

To account for missing data due to cloud cover, and satellite coverage, we applied a normalized factor to the fire count data to adjust for missing data. However this process does not account for no-data grid cells or data error conditions. The zero fire detection due to the lack of satellite information case, we used 3-day moving averages (only applied for zero-fire counts cells). If there was trouble in the satellite on-board system or at the receiving station, or if clouds persisted more than several days, the moving average scheme can not improve the AVHRR fire count data. In this case we used TOMS-AI data as an additional information source. However, the TOMS-AI data should be used with caution because it detects all (absorbing) aerosols, including dust and man-made smoke. So we applied several masks to help filter the information that is not caused by biomass burning. These masks include: 1) the classification of cloud conditions with and without rain using NCEP daily precipitation fields; 2) landcover maps to omit dust interference; and 3) maps of anthropogenic smoke sources including coal mine fires, oil wells, and gas drilling sites.

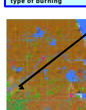

Landcover Fraction (Crop/Grass /Forest)

Emission Inventory Features

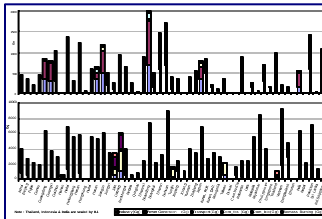

Regional emissions with sectoral contribution (Upper : SO_2, Lower : CO)

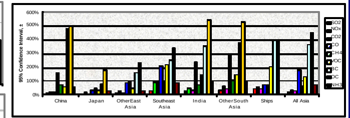

Uncertainty (%) in pollutant emission estimates (±95% confidence intervals)

We estimate the error for each emitting sub-sector by combining the coefficients of variation (CV, or the standard deviation divided by the mean) of the contributing factors. We then combine these uncertainties to estimate the uncertainty of emission estimates for each country. We tried wherever possible to use harmonized data across different source types and regions, even though the reporting practices of countries are not always consistent and available.

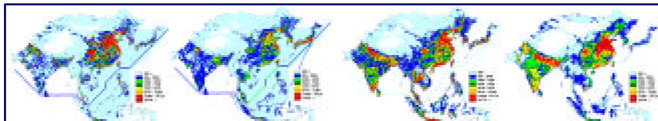

Area source emission distributions at 30 min grid resolution: SO_2 (leftmost), NO_x (middle left), NMVOC (middle right), and NH_3 (rightmost). The unit is Mg yr^{-1} per grid cell.

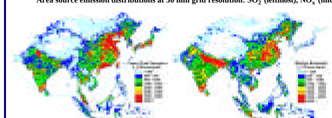

The same as above, but : CO from fossil fuel (left) and biofuel (right)

A number of features stand out: the source strengths of NH_3 in the agricultural areas of central China and northern India, the relatively strong signature of NO_x from transportation sources in Japan, significant emissions of NMVOC from biomass burning in Southeast Asia, and large SO_2 emissions in the Sichuan Basin and industrialized eastern China.

The CO from fossil fuel and biofuel combustion shows the contrast between source categories across developed and rural areas of China, where coal and biofuel combustion are prevalent.

The distributions of four NMVOC species shows the dominant source associations of these species: alkanes and ethene with biofuel combustion, toluene with industry, and formaldehyde with biomass burning. These maps are specifically for the month of January, and therefore they emphasize emissions from domestic heating in China and biomass burning in Southeast Asia

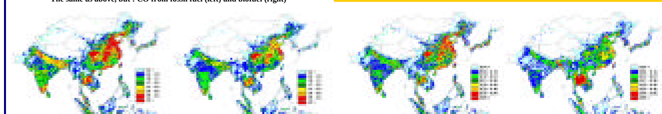

Area source emission at 30 min grid resolution: total alkanes (leftmost), ethene (middle left), toluene (middle right), and formaldehyde (rightmost). Unit : Moles/sec/grid

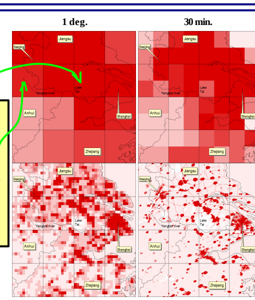

Lake Tai's effect can be seen at 30' × 30' resolution, but Yangtze River's effect cannot be clearly seen even in 5' × 5' resolution.

The initial allocation procedures are conducted at the highest possible resolution (30 sec × 30 sec—about 1 km × 1 km) then aggregated to lower resolution to meet the needs of modeling and analysis. In theory, any resolution is possible that is lower than or equal to 30 sec × 30 sec.

Left figure shows CO emission distributions at the 1 deg. (upper right), 30 min. (upper left), 5 min. (lower left), and 30 sec. (lower right) grid cell near Shanghai area. The effect of Lake Tai could be shown in 30 min. grid resolution, whereas Yangtze river is showed only with the highest resolution. In this figure, the effects of regional and sectoral differences can be clearly seen for the four different regions.

Right figure shows SO_2 (Upper) and CO (Lower) emission distributions at the highest resolution in the Pearl River Delta, as an example. In this figure, the effects of regional and sectoral differences can be clearly seen for the two different chemical species. This makes focused studies of large metropolitan air-sheds feasible with this inventory.

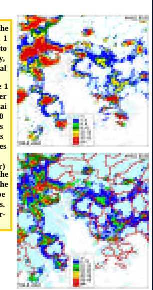

Emission-Based Analysis

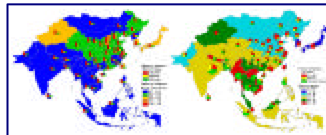

CO emissions by region and source-category overlayed with regional CO/CO_2 emission ratios (left), BC/OC emission ratio by regions overlayed with regional BC/OC ratios by source category (right).

Chemical groups identified from hierarchical cluster analysis

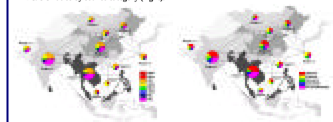

Source profiles from regional groups (left : major species, right : NMVOC species)

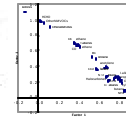

Chemical distributions identified in rotated factor space

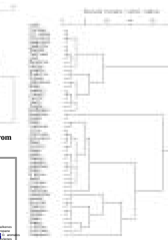

Regional groups identified from hierarchical cluster analysis

We analyzed regional and chemical characteristics using the region/chemical species information in our inventory.
From cluster analysis SO_2 shows up as a separate group. This reflects the fact that it is dominated by fossil fuel usage. NO_x, CO_2 and halocarbons are grouped as one, and they relate to the stage of development. CO, BC, OC, ethane, propane, ethene, propene, terminal alkenes, internal alkenes, and acetylene have similar regional distributions and are identified as a group. CH_4 and NH_3 are identified as a group and represent species not highly related to combustion. The hydrocarbon species are further clustered into four groups that reflect source category contribution. As an alternative analysis, we performed factor analysis using the rotated axis scheme. The factor loadings results are clustered into groups that are similar to those identified through the cluster analysis, and provide same confidence in the groups identified.
The results of regional cluster analysis reduced the 52 regions into 11 regional groups as shown in rightmost dendrogram Lower left figures show the emission profiles of the regional groupings.

Five DC8 flights (e.g. flight 6, 8, 9, 10, and 12) with 16 flight segments were selected as outflow events. Four chemical species (ethane, propane, butanes, and acetylene) out of 27 were selected as Chemical Mass Balance (CMB) model input. We analyzed spatial and temporally resolved emission data, backward trajectory analysis, 3D chemical source model, and wind field information to interpret source contribution from the CMB model for each selected outflow event.

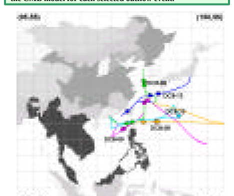

Selected DC8 flight and measurement points used in the analysis

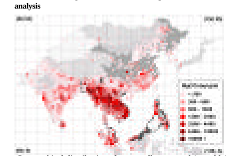

Geographical distribution of temporally averaged (monthly) biomass burning CO emissions

Evaluation measures of the CMB model estimates

Fl. No.	DATE	Time (GMT)	R^2	Ratio (Cal./Obs.)
DC8-06	3/4/2001	4.6	0.85	1.08
DC8-06	3/4/2001	5.2	0.84	1.01
DC8-06	3/4/2001	6.9	0.99	1.05
DC8-06	3/4/2001	7.0	0.98	1.03
DC8-08	3/9/2001	2.5	0.77	0.89
DC8-08	3/9/2001	3.3	0.99	0.95
DC8-08	3/9/2001	3.4	0.99	0.96
DC8-09	3/10/2001	3.3	0.88	1.16
DC8-09	3/10/2001	3.5	0.68	0.92
DC8-09	3/10/2001	5.2	0.68	0.92
DC8-09	3/10/2001	7.6	0.89	1.11
DC8-09	3/10/2001	7.9	0.89	1.11
DC8-10	3/13/2001	5.5	0.87	1.14
DC8-12	3/18/2001	3.5	0.92	0.94
DC8-12	3/18/2001	5.2	0.98	1.02
DC8-12	3/18/2001	5.7	0.88	1.11

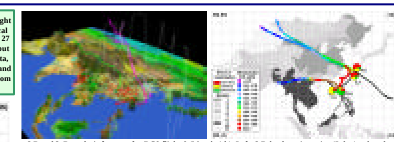

2-D and 3-D analysis features for DC8 flight 6 (March 4th). Left: 3-D back trajectories (5-day) colored with measured trace gas mixing ratio (light purple line: 4.6GMT, purple line: 5.2GMT, red line: 6.9GMT, green line: 7.0GMT); fossil fuel (light blue dots), biofuel (yellow dots), biomass burning (red dots) emissions; background map - topography colored by landcover. Right: Source sector contribution by CMB model and 5day 2-D back trajectories.

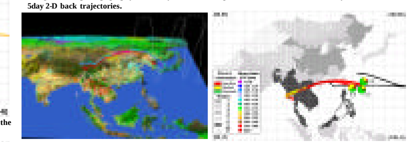

2-D and 3-D analysis features for DC8 flight8 (March 9th), Left: same as uppermost figure, but (light blue: 3.4GMT, purple: 3.3GMT, red: 2.5GMT); Right: same as uppermost figure.

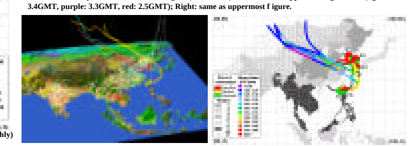

2-D and 3-D analysis features for DC8 flight9 (March 10th), Left: same as uppermost figure, but (light blue: 3.3GMT, red: 3.5GMT, light red: 5.2GMT, orange: 7.6GMT, yellow: 7.9GMT), Right: same as uppermost figure.

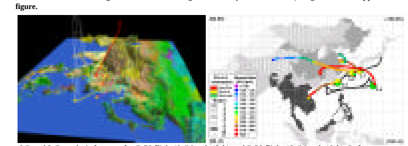

2-D and 3-D analysis features for DC8 flight10 (March 13th) and DC8 flight 12 (March 18th), Left: same as uppermost figure, but (yellow: flight10-5.5GMT, orange: flight12-3.5GMT, red: flight12-5.2GMT, purple: flight12-5.7GMT), Right: same as uppermost figure.

In general, Asian outflow is usually a complex mixture of biofuel, biomass and fossil sources. Flights in the post frontal regions at high latitudes and low altitudes were found to have a high contribution of fossil fuel emissions. Flights in the warm sector of cold fronts were dominated by biomass burning contributions (about 70%). Biofuel contributions were high (about 70%) when air masses come from central China. The receptor model results were shown to be consistent with 3D chemical model sensitivity studies for two common flight cases. Our receptor based approached showed consistency with biomass burning emission sensitivity tests using 3D chemical "source" models [Tang et al., 2002; Zhang et al., 2002].

In addition the results are consistent with source indicators. Ma et al., [2002] identified the contributions of bio-emission (e.g. biomass and biofuel) using the P-3B flight aerosol measurement data. They used dK^+/dSO_4^{2-} slopes from biomass(biofuel + biomass burning) and fossil plumes to analyze contribution of source categories. Both P-3B flight 10 and DC8 flight 8 flew a similar path along the 20° N latitude on the same day (March 9th). Their results using dK^+/dSO_4^{2-} slopes showed that the bio-emission contributed 80~100% of total mass. This result is consistent with ours, i.e. 87~96%.

The ratios of traditional source tracers including acetonitrile (CH_3CN : biomass combustion sources), tetrachloroethene (C_2Cl_4: fossil fuel sources) and SO_y (fossil fuel sources), and CO (general sources) were also analyzed. CH_3CN/SO_y ratios for the selected data points for DC8 flight 6 and flight 12 (high fossil fuel source contribution) showed lower values, whereas the selected data points for flight 8 (high biomass combustion source contribution) showed higher numbers. The SO_y/CO and C_2Cl_4/CO ratios were anti-correlated with CH_3CN/SO_y ratios for the same data points. The CMB receptor model, 3D chemical model and source tracer ratios showed consistent results for the selected flight cases.

References

Ma, Y., R. J. Weber, Y.-N. Lee, D. C. Thornton, A. R. Bandy, A. D. Clarke, D. R. Blake, G. W. Sachse, H. E. Fuelberg, J.-H. Woo, D. Streets, G. R. Carmichael, F. L. Eisele, The Characteristics and Influence of Biomass Burning Aerosols on Fine Particle Ionic Composition Measured in Asian Outflow During TRACE-P, *J. Geophys. Res.*, submitted in 2002.

Jung-Hun Woo, David Streets, Gregory R. Carmichael, Youhua Tang, Bongin Yoo, Won-Chan Lee, Narisara Thongboonchoo, Simon Pinnock, Gakuji Kurata, Itsushi Uno, Qingyan Fu, Stephanie Vay, Glen W. Sachse, Donald R. Blake, Alan Fried, D. C. Thornton, The Contribution of Biomass and Biofuel Emissions to Trace Gas Distributions in Asia during the TRACE-P Experiment, *J. Geophys. Res.*, submitted in 2002.

Streets, D. G., T. C. Bond, G. R. Carmichael, S. D. Fernandes, Q. Fu, D. He, Z. Klimont, S. M. Nelson, N. Y. Tsai, M. Q. Wang, J.-H. Woo, and K. F. Yarber, A year2000 inventory of gaseous and primary aerosol emissions in Asia to support TRACE-P modeling and analysis, *J. Geophys. Res.*, submitted in 2002.

Tang, Y., G. R. Carmichael, J.-H. Woo, N. Thongboonchoo, G. Kurata, I. Uno, and D. G. Streets, The Influences of Biomass Burning during TRACE-P Experiment Identified by the Regional Chemical Transport Model, *J. Geophys. Res.*, submitted in 2002.

Yarber, K.F., Streets, D.G., Woo, J.-H., and Carmichael, G.R., Biomass burning in Asia: annual and seasonal estimates and atmospheric emissions, *in preparation*, 2002.

Zhang, M., I. Uno, Z. Wang, H. Akimoto, G.R. Carmichael, Y. Tang, J.-H. Woo, D.G. structure of trace gas and aerosol distributions over the Western Pacific Ocean during TRACE-P, *J. Geophys. Res.*, submitted in 2002.

Acknowledgement : This work was supported by the NASA ACMAP and GTE Programs and the NSF Atmospheric Chemistry Program.